Flow Structure of a Fixed-frame Type Fire Whirl

MOHAMED I. HASSAN, KAZUNORI KUWANA, KOZO SAITO, and FENGJUAN WANG
Department of Mechanical Engineering
University of Kentucky
Lexington, KY 40506 USA

ABSTRACT

This paper reports the results of both experimental and numerical investigations on a laboratory-scale fixed-frame type fire whirl. We designed a fixed-frame type fire whirl generator consisting of two vertically oriented split PMMA cylinders which are placed in an off-center location to create a small compartment with a slit at each end. At the center of the compartment floor, a 5 cm-diameter 1-propanol pool fire generated upward buoyancy flow and fresh air entering the compartment through the slits, generating swirl motion in the compartment. This is a fixed-frame type fire whirl. We measured transient 2-D radial, tangential, and axial velocity profiles with 2-D particle image velocimetry (PIV). The radial and tangential velocity profiles were measured at four different heights (5, 10, 15, and 20 cm) along the axis of the fire whirl, while the axial velocity profiles were measured at 10 cm in the axial height. We also measured relative temperature distributions of the fire whirl with an infrared thermograph technique. These measurements show that both the tangential velocity and the absolute value of radial velocity increase with an increase in the radial distance, while they remain relatively constant along the axis. Our IR data also show that the relative temperature map stays unchanged along the axis. The radial locations where the maximum radial and tangential velocity were measured approximately coincide and are at about 3.5 cm on the radial coordinate, while the visible spinning flame location is at about 1.2 cm. This shows a difference in the velocity structure between open pool fires and fire whirls, because the location of the maximum flow velocity and visible flame approximately coincides for laminar open pool fires. A simple laminar 2-D axisymmetric CFD model was developed to simulate these measured flow and temperature structures created by the fire whirl, and reasonable agreement was obtained.

KEYWORDS: fire whirls, fire physics, particle image velocimetry (PIV), CFD

NOMENCLATURE LISTING

c_p	specific heat
D	diffusion coefficient
f	coupling function
g	gravitational acceleration
k	thermal conductivity
p	pressure
T	temperature (K)
r	radial coordinate
u_i	velocity component
W_i	molecular weight
Y_i	mass fraction
z	axial coordinate

Greek

α	angular velocity
β	thermal expansion coefficient
θ	tangential coordinate
ν	kinematic viscosity
ν_i	stoichiometric coefficient
ρ	density

subscripts

0	ambient
F	fuel
O	oxygen
P	products

FIRE SAFETY SCIENCE–PROCEEDINGS OF THE EIGHTH INTERNATIONAL SYMPOSIUM, pp. 951-962

INTRODUCTION

Structures of fire whirls are of current interest both in practical terms, for fire safety issues related to the inherently fast spreading rate and increased radiant emission from flame, and in terms of a fundamental curiosity about its complex mechanism [1-5]. Under extreme condition, a fire whirl was responsible for 38,000 deaths caused by The Great Kanto Earthquake that struck the downtown Tokyo area in 1923 [6]. Soma and Saito [6] collected a historical record of large scale fire whirls and categorized them into three different types. Pitts [3] provided a comprehensive review on wind-aided fires and included fire whirls in his review. These studies clearly indicate the very complex nature of fire whirls observed during forest, urban and building fires.

Two different approaches can be recognized in the past studies on fire whirls. The first approach might be to study a specific example of a large scale fire whirl observed during mass fires using scale model experiments or numerical simulations. This approach requires some guess work because there are no reliable velocity measurement data that can specify structures of the fire whirl. Difficulty of the measurement lies in that the fire whirls associated with large scale mass fires appear without warning and when they occur, they may only last for seconds to no more than a few minutes [6,7]. Access to those fire whirls for measurement would be both highly fortuitous and highly dangerous.

The second approach might be to create fire whirls in the laboratory under well controlled boundary conditions and study them thoroughly. This second approach allows researchers to conduct a series of reliable measurements on the thermal and fluid dynamic structures of fire whirls.

Taking the second approach, in this paper we created a fixed-frame type fire whirl in the laboratory and measured transient 2-D radial and tangential velocity profiles in and around the fire whirl using 2-D component particle image velocimetry (PIV). Infrared thermograph (non-intrusive) technique was used to measure relative temperature distributions of the fire whirl, since any intrusive techniques including thermocouple can change the fire-whirl-generated flow and temperature fields and thus are not acceptable.

Another type of fire whirls created in the laboratory, known as Emmons type, have structures assumed to be different from the fixed-frame type, but so far no clear comparison has been made in terms of their measured flow structures. In this study, we chose to study the fixed-frame type, because it represents frequently observed fire whirls during urban and building fires where building and room walls provide favorable geometry for inducing whirling flow. However, comparison of both types of fire whirl would be beneficial in order to study fire whirls, so we review the past studies on both types. Note that we have already obtained PIV flow measurement data for the Emmons type fire whirl, but the results are not included here due to page limitation and will be reported in the future.

Emmons and Ying [1] are pioneers who created an Emmons type fire whirl with a rotating disc surrounded by a fine mesh screen and placed a 10 cm-diameter acetone pool fire at the center of the disc. The pool fire produced the buoyancy-driven upward flow; fresh air entered the compartment through the screen rotating with the table, generating swirl motion in the compartment. They measured temperature profiles with a fine thermocouple, but no velocity profiles were obtained, due possibly to difficulties in measuring spinning fires and created spinning flow field through a rotating cage. Battaglia *et al.* [8] proposed a simplified model that can describe an interaction between

circulation and buoyant convection and showed that the model could capture many aspects of experimental results. They also numerically simulated the behavior of fire plumes arising from an Emmons type fire whirl by imposing circulation with a large eddy simulation (LES) turbulent model [9]. Their calculated velocity profiles were, however, not validated against experimental data because no velocity measurement data are available for Emmons type fire whirls.

For the study on fixed-frame fire whirls, Saito and Cremers [10] used two vertically oriented rectangular screens to create a small compartment with a slit at each end. At the center of the compartment floor, a small pool fire generated upward buoyancy flow; fresh air entered the compartment through the slits, generating swirl motion in the compartment. Satoh and Yang [11,12] designed a laboratory-scale fixed-frame type fire whirl experiment, made several interesting observations on behavior of fire whirls, and mentioned velocity profiles at several different points including near the tip of one of their fire whirls. But they did not measure radial and tangential velocity profiles in and around the fire whirl. They also simulated the temperature and velocity fields created by a fixed frame type fire whirl by using a no-flame transient 3-D square enclosure model and compared their predictions to the corresponding measurement. Comparison between the prediction and the measurement, however, is qualitative at best due to the lack of well established velocity profile data.

These past studies suggest that we still do not completely understand the detailed thermal and fluid dynamic structures of both Emmons type and fixed-frame type fire whirls. The major cause is lack of accurate and reliable (radial and tangential) velocity profile data in and around fire whirls of each type. Here we focus on the detailed flow measurement of a fixed frame type fire whirl. In addition, we obtained IR temperature map on the fire whirl and a simple model to calculate both flow and temperature fields.

EXPERIMENTAL METHODS

Fire Whirl Generator

Figure 1 shows a schematic of our fixed-frame type fire whirl generator, infrared thermograph and PIV system, and Fig. 2 shows two photographs of a fixed-frame type fire whirl (Fig. 2a shows an overall shape and Fig. 2b shows an enlarged flame base). The fixed frame-type fire whirl generator is similar to the one employed in [10], where two rectangular screens instead of the current two split cylinders (diameter, 30 cm) were used. By using split cylinders, the velocity field is expected to be more axisymmetric, helping to obtain a fundamental understanding of velocity field. At the center of the cylinders, a shallow 5 cm–diameter 1-propanol pool fire was placed. Compartment slit distance was changed from 0 (no fire whirl) to 4 cm to experimentally obtain the most stable fire whirl generation condition, the slit distance of 2 cm. 1-propanol was chosen because it emits less soot, a favorable condition for PIV measurement in comparison to sooty hydrocarbon fuels, and also because it can represent structures of light-soot hydrocarbon and alcohol pool fires [13].

PIV System and Velocity Measurement

Since general theory and procedures for PIV system are detailed in [14], here we only provide a summary of key features of the PIV system whose schematic is shown in Fig. 1. PIV technique requires the to-be-measured flow-field to be seeded. The flow

around the fire whirl was seeded with a few μm-diameter smoke particles provided by a smoke generator and with 3-4 μm diameter silica particles.

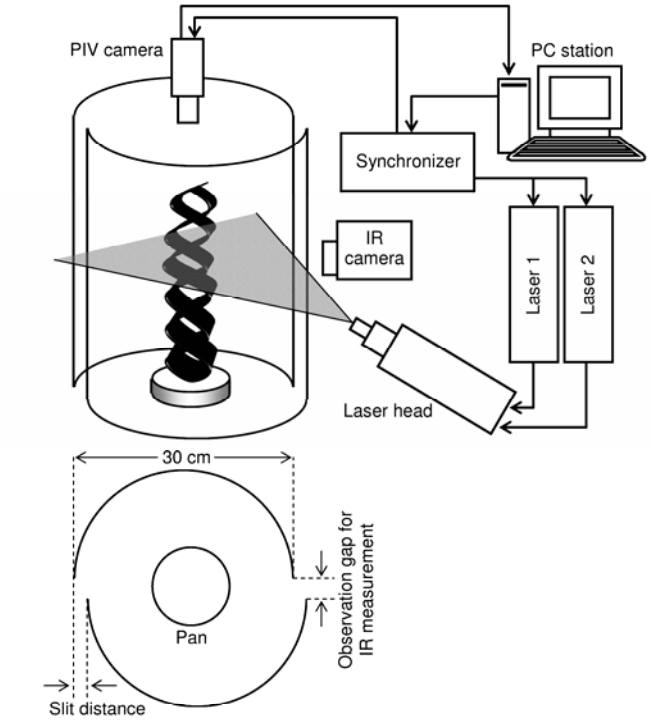

Fig. 1. A schematic of fixed-frame type fire whirl generator with PIV system and IR camera.

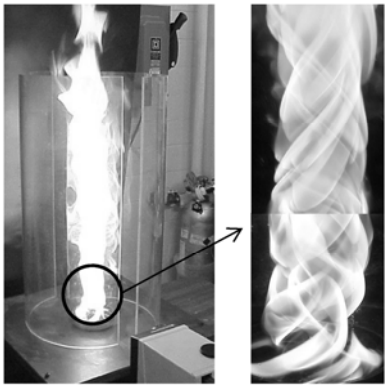

(a) (b)

Fig. 2. Photographs of a fixed-frame type fire whirl induced by a 5 cm-diameter 1-propanol pool fire: (a) an overall image, (b) an enlarged image of the flame base structure.

Our PIV system consists of three main units: two Nd:YAG (532 μm wave length) pulse lasers, an image capturing unit, and a computing and display unit. These units are well synchronized using a signal synchronizer. The laser light reflected by the particles was recorded using a 30-frame-per-second cross-correlation CCD camera on a two-frame straddle, one frame for each pulse. Cross CCD camera allows a frame straddling pair of images to be captured less than 300 μs after an external trigger signal is used, effectively. In frame straddling the laser is pulsed at the end of the first exposure period and then at the start of the second exposure period. The PIV parameters, such as laser pulse rate, pulse separation time, laser light energy intensity, and particle density and diameter, were experimentally determined to optimize the PIV image resolution and accuracy of the data.

Velocity measurements were conducted at four different axial heights (at z = 5, 10, 15, and 20 cm); the obtained velocity profiles were very similar at all four different heights.

IR Temperature Measurement

An infrared camera (detector wavelength: 4-12 μm, response time: 10-1 s, temperature resolution: 0.5°C, spatial resolution: 0.2 mm) was used to qualitatively assess relative temperature distributions of the whirling flame. To determine the emissivity set up for the IR camera, we employed a 1-propanol open pool fire under quiescent laboratory conditions and measured its temperature with a 50 μm diameter Pt-Pt/Rh thermocouple with a 0.5 mm ball head. The emissivity, 0.92 for the IR camera, gave us good agreement between the two readings and that emissivity was used for our IR temperature measurement for the fire whirl through an observation gap, shown in Fig. 1, to avoid radiation absorption by the PMMA wall. Note that these IR temperature data are an integrated IR signal along the line of sight, and do not represent absolute flame temperatures. They only indicate relative temperature changes in a qualitative manner. The IR temperature image can be valuable data (as demonstrated for a large scale pool fire test) to identify the relative temperature change in the flame [15]. Here we use IR data only for that purpose.

EXPERIMENTAL RESULTS

Figure 2a shows a photograph of a fixed-frame type fire whirl. With a fire whirl, typically the flame significantly increases its visible length and constricts its diameter. Those characteristics agree with experimental observations made by Emmons and Ying [1], Satoh and Yang [11,12] and numerical predictions by Battaglia *et al.* [8,9], suggesting that the buoyancy/shear-flow interaction allows more air to penetrate into the flame zone for stretching the flame. Note that under our experimental conditions, both types (Emmons and fixed-frame) have laminar flame in the region close to the fuel pan as shown in Fig. 2b.

Figure 3 shows tangential and radial velocity distributions of a 5-cm diameter 1-propanol pool-fire-induced fixed-frame type fire whirl at four different axial heights (z = 5, 10, 15, and 20 cm). The approximate location of the visible flame is shown by the broken line. The axial velocity profile along the radial direction at z = 10 cm is also included in the figure. The maximum radial and tangential velocity were measured at about the radial

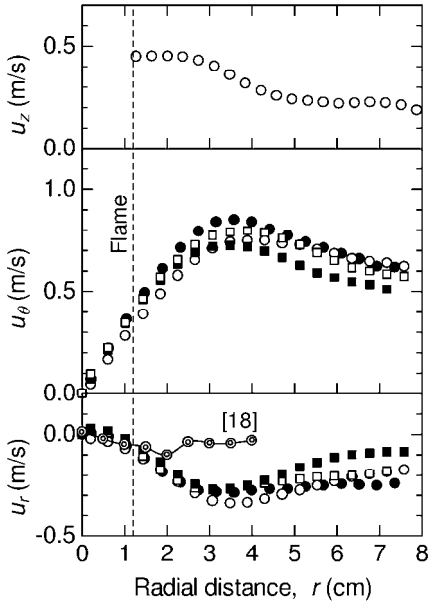

Fig. 3. PIV measured axial, tangential, and radial velocity distributions of a fixed-frame type fire whirl induced by a 5 cm-diameter 1-propanol pool-fire at four different axial heights (5, 10, 15, and 20 cm). Symbols: ● at z = 5 cm; ○ at z = 10 cm; ■ at z = 15 cm; □ at z = 20 cm. Radial velocity distribution of pool fire without swirl at z = 10 cm in [18] is also plotted.

Coordinate = 3.5 cm, while the visible flame location is at about 1.2 cm. Note that our PIV measurements at the radial distance larger than 3.5 cm are expected to be accurate, while for $0 < r < 3.5$ cm they are not accurate due to evaporation of the seeding particles. This shows some differences in the velocity structure between open pool fires and fire whirls, because the location of the maximum flow velocity and visible flame approximately coincides for laminar open pool fires [13,16,17,18]. The PIV radial velocity distribution by Gore *et al.* [18] for a 7.1 cm diameter methane/air open pool fire (without swirl) at z = 5 cm is also added in the figure. With a fire whirl, the radial inflow increased and its peak location shifted outside. Obtained tangential velocity has a typical Rankine-type radial distribution, observed also for a large scale moving type fire whirl [6], where it increases linearly from zero to the maximum value in the interior region and decreases with radius in the outer region. Tangential velocity distribution of this type is characterized by its maximum value and core radius. Tangential velocity distributions at all the heights have maximum value of 0.7 to 0.9 m/s and core radius of 3 to 4 cm, and no significant changes were found at different heights, indicating that the air-entrainment velocity along the slit is uniform. More accurate velocity measurement for the region $0 < r < 3.5$ cm should be conducted in the future. Therefore, further detailed discussion on our PIV measurement data is not available here.

Figure 4a shows infrared thermal image of the fire whirl corresponding to the PIV measured fire whirl. It can be seen that the temperature field is fairly uniform in the axial direction, showing that the uniform distributions of tangential velocity and radial velocity (Fig. 3) are induced by this uniform temperature distribution.

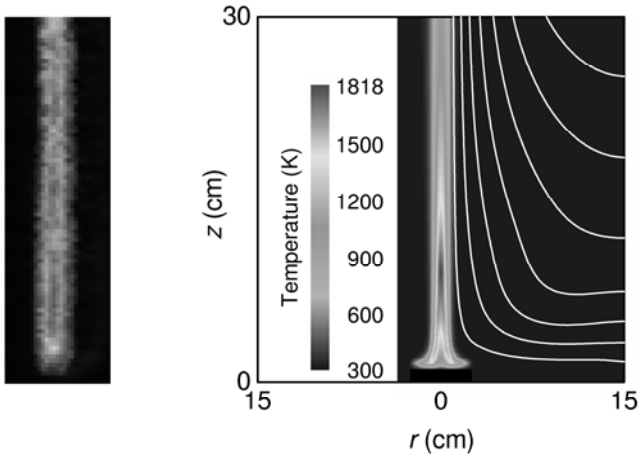

(a) (b)

Fig. 4. Temperature distributions of a 5 cm-diameter 1-propanol pool-fire-induced fixed-frame type fire whirl: (a) the measured IR temperature map (b) model simulation. The simulated temperature field and streamlines are for $\alpha = 0.2$ rad/s, and the contour line of stream function starts from 5×10^{-5} kg/s with an interval of 5×10^{-5} kg/s.

MODELING OF FLAME-SWIRL INTERACTION

A series of computational fluid dynamics (CFD) simulations were conducted to understand the interaction between flame and swirl flow. For better understanding of fundamental mechanism of the interaction, we have developed a simplified model that can predict fluid dynamic structure of fire whirl with reasonable accuracy. Because of split cylinders' configuration of our fire whirl generator (Fig. 1), the fixed-frame type fire whirl is essentially a 3-D phenomenon. However, our PIV measurement showed a well organized axisymmetric flow structure which can be accurately simulated with 2-D modeling. Since laminar flame was observed in the region close to the fuel pan as shown in Fig. 2b, we treat the fire whirl as a wrinkled laminar flame (estimated Re ≈ 1000). A schematic diagram of our model is shown in Fig. 5, where the radius of computational domain (R) is based on our fixed-frame type fire whirl generator (Fig. 1a). The height of the computational domain is 300 cm in order to minimize the effect of the top boundary. Major assumptions adopted here are summarized below:

(a) Flow is laminar, steady, and axisymmetric ($\partial/\partial\theta = 0$).

(b) Density is constant except for the buoyancy term in the z-momentum equation (Boussinesq approximation).

(c) Gas properties are constant.

(d) Le = 1, i.e., $k / \rho c_p = D$.

(e) The rate of reaction (one-step irreversible reaction: $F + \nu_O O \rightarrow \nu_P P$) is infinitely rapid.

(f) The velocity at the liquid surface due to evaporation is proportional to heat flux at the liquid surface (Fig. 5).

(g) Temperature and fuel mass fraction at the liquid surface are constant.

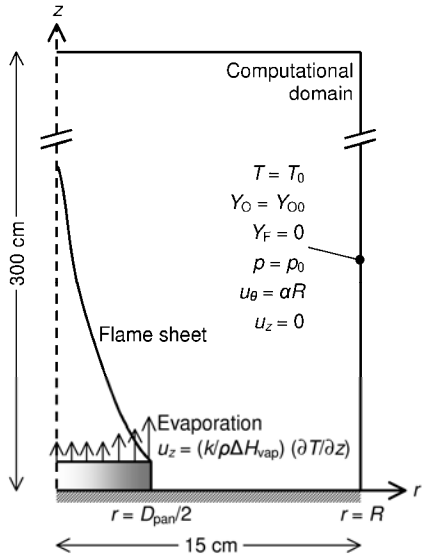

Fig. 5. A schematic diagram of our numerical model.

Based on above assumptions, the governing equations are as follows:

$$\frac{1}{r}\frac{\partial}{\partial r}(ru_r)+\frac{\partial u_z}{\partial z}=0 \tag{1}$$

$$u_r\frac{\partial u_r}{\partial r}-\frac{u_\theta^2}{r}+u_z\frac{\partial u_r}{\partial z}=-\frac{1}{\rho}\frac{\partial p}{\partial r}+\nu\left[\frac{\partial}{\partial r}\left(\frac{1}{r}\frac{\partial}{\partial r}(ru_r)\right)+\frac{\partial^2 u_r}{\partial z^2}\right] \tag{2}$$

$$u_r\frac{\partial u_\theta}{\partial r}+\frac{u_r u_\theta}{r}+u_z\frac{\partial u_\theta}{\partial z}=\nu\left[\frac{\partial}{\partial r}\left(\frac{1}{r}\frac{\partial}{\partial r}(ru_\theta)\right)+\frac{\partial^2 u_\theta}{\partial z^2}\right] \tag{3}$$

$$u_r\frac{\partial u_z}{\partial r}+u_z\frac{\partial u_z}{\partial z}=-\frac{1}{\rho}\frac{\partial p}{\partial z}+\nu\left[\frac{1}{r}\frac{\partial}{\partial r}\left(r\frac{\partial u_z}{\partial r}\right)+\frac{\partial^2 u_z}{\partial z^2}\right]+\beta(T-T_0)g \tag{4}$$

$$u_r\frac{\partial f_1}{\partial r}+u_z\frac{\partial f_1}{\partial z}=D\left[\frac{1}{r}\frac{\partial}{\partial r}\left(r\frac{\partial f_1}{\partial r}\right)+\frac{\partial^2 f_1}{\partial z^2}\right] \tag{5}$$

$$u_r \frac{\partial f_2}{\partial r} + u_z \frac{\partial f_2}{\partial z} = D\left[\frac{1}{r}\frac{\partial}{\partial r}\left(r\frac{\partial f_2}{\partial r}\right) + \frac{\partial^2 f_2}{\partial z^2}\right] \quad (6)$$

Here, scalar variables, f_1 and f_2, are defined as:

$$f_1 = Y_O - \frac{W_O}{W_F}\frac{\nu_O}{\nu_F}Y_F, \quad f_2 = T - \frac{\Delta H_{comb}}{c_p}Y_F \quad (7)$$

Since the change of tangential velocity in the *z*-direction is negligible in comparison with that in the *r*-direction as shown in Fig. 3, a constant tangential velocity, αR (α: angular velocity), was imposed at $r = R$. By changing the value of α, the effect of swirl intensity on generated fire whirl can be examined. To solve the above governing equations, a commercial CFD software package (Fluent, Fluent Inc.) with user-defined scalar and subroutine functions was used. The size of the computational mesh used for our simulations is 1 mm (*r*) × 2 mm (*z*).

Predicted temperature and velocity fields for $\alpha = 0.2$ rad/s are shown in Fig. 4b. Predicted tangential velocity showed a distribution similar to our observation (Fig. 3). Two characteristic parameters of the tangential velocity distribution, maximum velocity ($u_{\theta max}$) and core radius (c), are plotted as a function of swirl intensity (α) in Fig. 6. With an increase in swirl intensity, maximum tangential velocity linearly increases and core radius stays almost constant, with a slight decrease. These results indicate that the tangential velocity normalized by its maximum value has an identical distribution. Distributions of normalized tangential velocity and radial velocity at $z = 10$ cm are shown in Fig. 7. Similar measurements were done at four different heights (5, 10, 15, and 20 cm); all the results showed similar trends to Fig. 7. Fire whirl experiments showed that the flow structure near the flame base was laminar, while the flow structure becomes turbulent in the upper region of flame. To simplify the problem, however, we treated the entire flame as laminar based on the study by Baum *et al.* [19] and used the Boussinesq approximation. Our aim here is to see whether or not our model can explain the trend of experiments, but not quantitative agreement with the experimental data. When the trend agrees as shown in Fig. 7, our model is successful in capturing the essence of fluid dynamics of flame-swirl interactions.

CONCLUSIONS

We measured transient 2-D radial and tangential velocity profiles at four different heights along the axis of a fixed-frame type fire whirl. In addition, we obtained an infrared image of the whirling flame and developed a simple laminar 2-D model (based on observed flame base structure) to simulate the measured velocity distributions and the observed temperature field. Our PIV measurement showed axisymmetric flow pattern, where the tangential velocity component was larger than radial velocity component. Fire whirl created its own unique tangential velocity and also helped increase the radial inflow about three times at its peak value compared to an approximately same diameter open pool fire (without swirl). The radial velocity profile and the tangential velocity profile each had a very similar profile along the fire whirl axis and the IR measured relative temperature map indicated there is no significant temperature change along the fire whirl

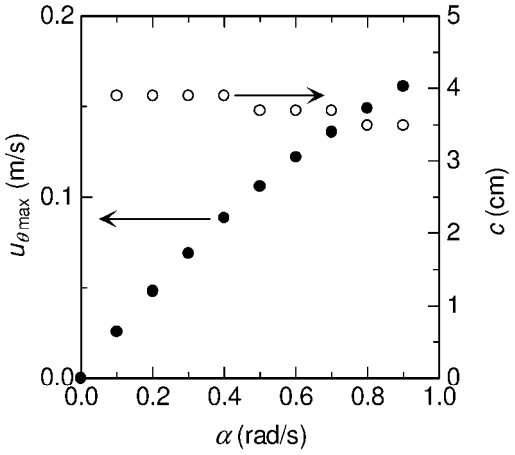

Fig. 6. Calculated maximum tangential velocity ($u_{\theta\max}$) and the core radius (c) as a function of swirl intensity (α).

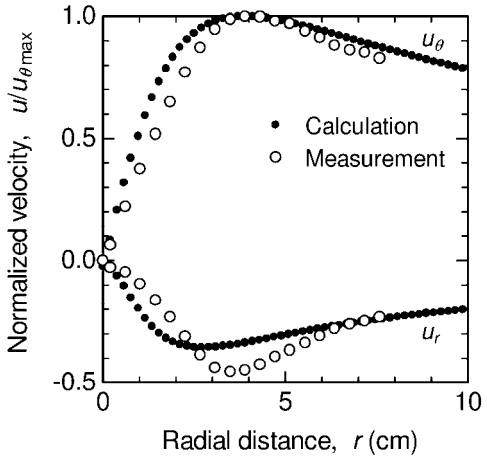

Fig. 7. Calculated distributions of tangential velocity and radial velocity (pan diameter: 5 cm, the axial height: 10 cm, and α = 0.2 rad/s).

axis. There is qualitative agreement between the calculated and measured velocity profiles, indicating the proposed simple laminar model may capture the flow characteristics.

ACKNOWLEDGEMENTS

This study was supported in part by NASA (NAG3-2567) and in part by Kentucky Science and Technology Foundation. We would like to acknowledge F. Battaglia, R.G. Rehm, and H.R. Baum for their valuable discussions and comments on fluid dynamic structures of fire whirls.

REFERENCES

[1] Emmons, H.W., and Ying, S.J., "The Fire Whirl," *Proc. Combust. Inst*, **11**, pp. 475-488, (1967).

[2] Williams, F.A., "Urban and Wildland Fire Phenomenology," *Prog. Energy Combust. Sci.*, **8**, pp. 317-354 (1982).

[3] Pitts, W.M., "Wind Effects on Fires," *Prog. Energy Combust. Sci.*, **17**, pp. 83-134, (1991).

[4] Hirano, T., and Saito, K., "Fire Spread Phenomena: The Role of Observation in Experiment," *Prog. Energy Combust. Sci.*, **20**, pp. 461-485, (1994).

[5] Bég, O.A., Bég, T.A., and Takhar, H.S., *Fluid Mechanics of Swirling Flames and Fire Whirls*, WIT Press (to appear).

[6] Soma, S., and Saito, K., "Reconstruction of Fire Whirls Using Scale Models," *Combust. Flame*, **86**, pp. 269-284, (1991).

[7] Countryman, C.M., "Project Flambeau - An Investigation of Mass Fire (1964-1967)," Vol. I, *Final Rep. Office of Civil Defense Order No. OCD-PS-65-26*, Pacific Southwest and Range Experimental Station, U.S. Forest Service, 1969.

[8] Battaglia, F., Rehm, R.G., and Baum, H.R., "The Fluid Mechanics of Fire Whirls: An Inviscid Model," *Physics of Fluids*, **12**, pp. 2859-2867, (2000).

[9] Battaglia, F., McGrattan, K.B., Rehm, R.G., and Baum, H.R., "Simulating Fire Whirls," *Combustion Theory and Modelling*, **4**, pp. 123-138, (2000).

[10] Saito, K., and Cremers, C.J., "Fire-whirl Enhanced Combustion," *Proc. Joint ASME/JSME Fluid Engineering Conference*, Hilton Head, 1995.

[11] Satoh, K., and Yang, K.T., "Experimental Observations of Swirling Fires," *ASME Heat Trans. Div.*, **335**, pp. 393-400, (1996).

[12] Satoh, K., and Yang, K.T., "Simulations of Swirling Fires Controlled by Channeled Self-generated Entrainment Flows," *Proceedings of the Fifth International Symposium*, International Association for Fire Safety Science, 1997, pp. 201-212.

[13] Venkatesh, S., Ito, A., Saito, K., "Flame Base Structure of Small-scale Pool Fires," *Proc. Combust. Inst.*, **26**, pp. 1437-1443, (1996).

[14] Raffel, M., Willert, C., and Kompenhans, J., *Particle Image Velocimetry*, Springer, 1998.

[15] Koseki, H., "Large Scale Pool Fires: Results of Recent Experiments," *Proceedings of the Sixth International Symposium*, International Association for Fire Safety Science, 2000, pp. 115-132.

[16] Zhou, X.C., Gore, J.P., and Baum, H.R., "Measurements and Prediction of Air Entrainment Rates of Pool Fires," *Proc. Combust. Inst.*, **26**, pp. 1453-1459, (1996).

[17] Zhou, X.C., and Gore, J.P., "Experimental Estimation of Thermal Expansion and Vorticity Distribution in a Buoyant Diffusion Flame," *Proc. Combust. Inst.*, **27**, pp. 2767-2773, (1998).

[18] Xin, Y., Gore, J., McGrattan, K.B., Rehm, R.G., and Baum, H.R., "Large Eddy Simulation of Buoyant Turbulent Pool Fires," *Proc. Combust. Inst.*, **29**, pp. 259-266, (2002).

[19] Baum, H.R., and Rehm, R.G., *Twenty-eighth International Symposium on Combustion*, Edinburgh, 2000, (in poster presentation).